Pergamon

Tetrahedron 56 (2000) 1429–1436

TETRAHEDRON

Theoretical Study on the Reactivity of Phenyl Cation with a Propyl Group at *Ortho*-Position

Kenzi Hori,[a,*] Takaaki Sonoda,[b] Masayuki Harada[b] and Suzuko Yamazaki-Nishida[c]

[a]*Department of Applied Chemistry and Chemical Engineering, Yamaguchi University, Ube 755-8611, Japan*
[b]*Institute of Advanced Material Study, Kyushu University, Kasuga 816-8580, Japan*
[c]*Department of Chemistry, Faculty of Science, Yamaguchi University, Yamaguchi 753-8512, Japan*

Received 2 November 1999; accepted 6 January 2000

Abstract—Photosolvolysis of 2-chloropropylbenzene in trifluoroethanol (TFE) produces propylbenzene, indane, 2-trifluoroethoxypropylbenzene and other solvolysis products. Propylbenzene clearly comes from 2-propylphenyl radical intermediate while the other products suggest existence of 2-propylphenyl cation as an intermediate. Density functional theory (DFT) calculations at the B3LYP/6-31G** level of theory were carried out to research reaction paths for the solvolysis products through the cationic intermediate. Three paths investigated in the present study well explain the products obtained in our experiments. The DFT calculations strongly suggest existence of the phenyl cation as an intermediate in the photosolvolysis of 2-chloropropylbenzene in TFE.

Introduction

The chemistry of the phenyl cation is little known in comparison with other common carbocations because of its thermodynamic instability and high reactivity[1] although there are many theoretical and experimental investigations which have brought this unstable intermediate into focus. Theoretical investigations on the electronic structure of phenyl cation[2] indicated that the molecular plane of the phenyl cation, being in singlet ground state, has a vacant orbital which is orthogonal to the π system of the aromatic ring and is incapable of obtaining conjugative stabilization as shown below.

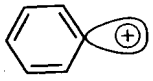

Many experimental efforts have been made to obtain insight into the electronic structure and reactivity of phenyl cations in solution. The cations, which are formed as metastable intermediates in dediazoniation of benzenediazonium ions, attracted considerable interest in the 1970s. It is because benzenediazonium ions are only the aromatic species of a precursor of the phenyl cation.[3] Martinson et al. produced phenyl cation with a propyl side-chain by dediazoniation of 2-propylbenzenediazonium tetrafluoroborate in aqueous sulfuric acid. The major products of the reaction were indane and 2-propylphenol.[4] Furthermore, it was reported that various isomeric olefins, alcohols and indane derivatives were also produced in dediazoniation reaction of 2-butylbenzenediazonium ion.[5] The phenyl cation can be an intermediate of these reactions.

After triflate and related 'super' leaving groups in the S_N1 solvolysis reactions were known to generate highly destabilized alkyl and vinyl cations, several unsuccessful attempts were made to generate phenyl cations as metastable intermediates by using methods other than dediazoniations.[6] A sole example of the solvolysis of phenyl triflates with trimethylsilyl groups on both *ortho*-positions in fluorinated solvents has been reported to generate 2,6-bis(trimethylsilyl)phenyl cation which is highly stabilized by hyperconjugation with the silyl groups.[7] Several investigations have successfully told us that the radiochemical decay of tritiated compounds is the unique method for generating phenyl cations from tritiated benzenes in the gas phase and solution.[8]

Photosolvolysis was also attempted in order to generate the very unstable intermediate. An S_N1 Ar* mechanism via phenyl cations has been proposed so as to account for the behavior of chlorobenzenes in nucleophilic photosubstitution reactions as one of several possible reaction mechanisms.[9] Recently, we also performed photosolvolysis of 2-chloropropylbenzene **1** in trifluoroethanol (TFE) and obtained the results which are summarized in Eq. (1).

Propylbenzene **2**, indane **3** and the solvolysis products **4**–**7** were made together with small amounts of olefins **8** and **9**.[10] It is not so surprising that **2** is formed in this reaction

Keywords: carbenium ions; solvent and solvent effect; solvolysis; theoretical studies.
* Corresponding author. Tel.: +81-836-35-9045; fax: +81-836-35-9933; e-mail: kenji@sparklx.chem.yamaguchi-u.ac.jp

0040–4020/00/$ - see front matter
PII: S0040-4020(00)00028-4

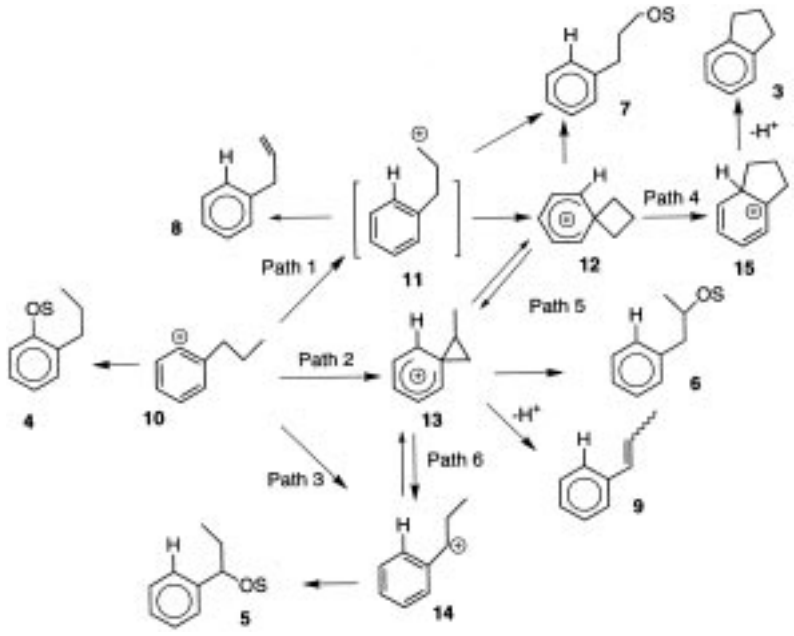

Scheme 1.

because this product indicates a mechanism through a radical intermediate: the homolytic fission of a carbon–halogen bond in **1** produces 2-propylphenyl and Cl radicals, and then, the 2-propylphenyl radical abstracts an H radical from a solvent to form **2**. However, **3** and **4** are similar products as dediazoniation of 2-propylbenzenediazonium ion produces. Moreover, **5**–**9** are also solvolysis or deprotonated products derived from intermediates with a cation center in the side chain shown in Scheme 1. It is quite unusual to see these compounds in the products of photosolvolysis of **1**.

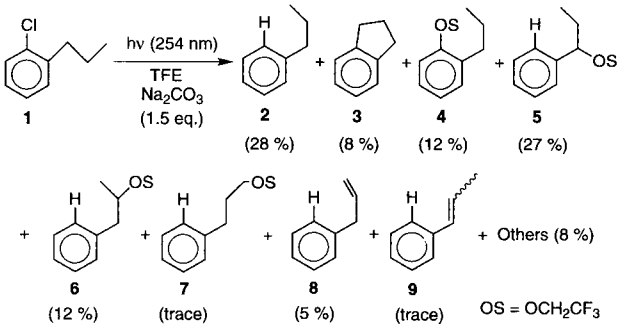

(1)

The use of TFE provides a key to obtaining these solvolysis products. In a solvent with poor nucleophilicity, electron transfer occurs from 2-propylphenyl to the Cl radical and forms an intermediate 2-propylphenyl cation **10**. If this is correct, we can draw Scheme 1 which represents feasible routes producing solvolysis products observed in our experiments.

It is not difficult to expect the formation of solvolysis product **4** by reaction of **10** with a solvent. The cationic carbon in the benzene ring of **10** accepts a hydride at the γ-carbon of the propyl side-chain to generate intermediate **11**, followed by intramolecular cyclization to form a spiro intermediate **12** (Path 1). Nucleophilic attack of solvent causes **11** or **12** to yield **7**. Deprotonation from the β-carbon of **11** produces **8**. Isomerization of **12** is promoted due to relief of strain energy in the four-membered ring, leading to formation of **15**, the precursor of **3** (Path 4). It is also possible to consider a route (Path 5) where **12** isomerizes to **13** and vice versa due to migration of a hydride between the β- and the γ-carbons of the side chain.

A phenonium intermediate **13** is involved in Path 2 where a hydride of the β-carbon in the propyl side chain shifts to the cationic carbon of the benzene fragment in **10**. The loss of H^+ from this intermediate produces **9** with an olefin fragment in the side chain although its product ratio is almost negligible. A hydride transfer from the α- to the β-position in the side chain of **13** gives the benzyl cation **14** (Path 6) which is considered to be relatively stable among intermediates in Scheme 1. The same intermediate is also generated directly from **10** (Path 3). These intermediates, **13** and **14**, react with solvents to produce solvolysis products **6** and **5**, respectively.

Many factors determine the course of the photochemical aromatic substitution reactions even though the detailed analysis of products suggests the reaction mechanisms through the phenyl cation **10** shown in Scheme 1. No direct spectroscopic observations of metastable phenyl cations in solution have been made in the present reaction. It is very difficult to prove the scheme experimentally because all the intermediates are unstable. Theoretical calculations are powerful tools for investigating such mechanisms in which reactants and intermediates are too unstable. In the present study, density functional theory (DFT) calculations at the B3LYP/6-31G** level of theory were applied to examine Scheme 1 of the photosolvolysis from 2-chloropropylbenzene in TFE.

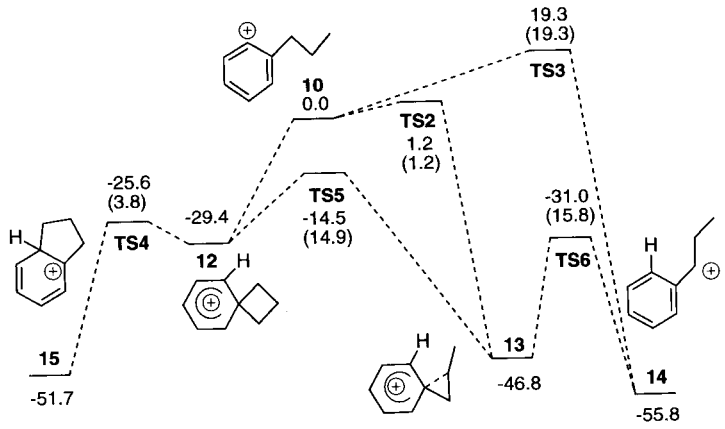

Figure 1. Energy-level diagram relative to the phenyl cation **10** as the feasible intermediate in kcal mol^{-1} unit. Values in parentheses are activation energies for each path.

Method of Calculation

The DFT calculations were carried out by the gaussian94 program on both the NEC HSP computer at the Institute for Molecular Science and workstations of our laboratory.[11] We used B3LYP/6-31G** level of theory[12] for geometry optimizations. The energy gradient method was used to optimize molecular geometries including transition states (TSs). All the optimized geometries were checked by looking through vibrational frequency calculations.

Fig. 1 displays the energy relation among intermediates and TSs whose optimized geometries are summarized in Fig. 2. Table 1 lists both energy differences relative to that of **10** or **13**+MeOH and activation energies for the corresponding routes of the reactions. Performing the intrinsic reaction

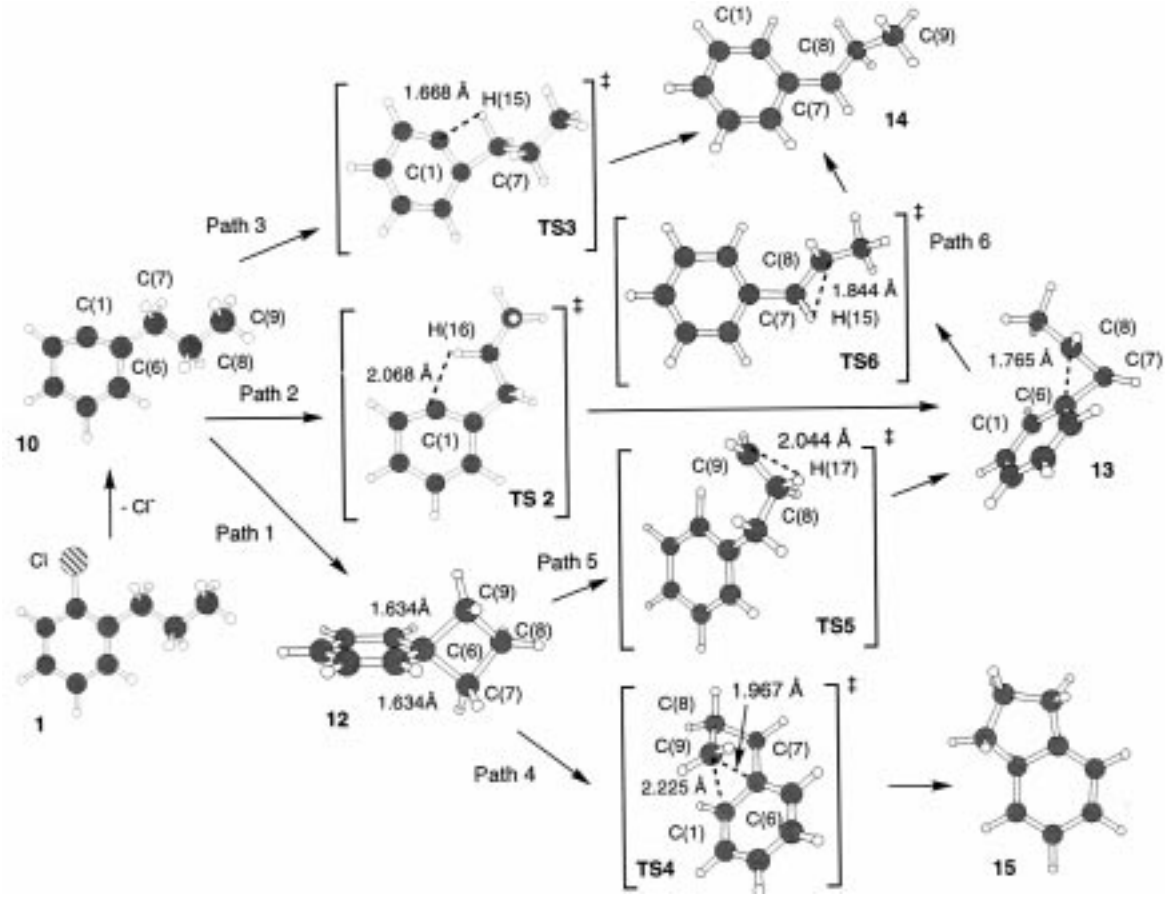

Figure 2. Optimized structures of reactants, intermediates and TSs for giving solvolysis products.

Table 1. Total energies, energy differences relative to that of **10** or **13**+MeOH and activation energies for the corresponding routes

Molecule	ΔE (kcal mol^{-1})[a]	Total energy (Hartree)
10	0.0	−349.23938
12	−29.4	−349.28627
13	−46.8	−349.31394
14	−55.8	−349.32825
15	−51.7	−349.32171
TS2	1.2 (1.2)	−349.23741
TS3	19.3 (19.3)	−349.20865
TS4	−25.6 (3.8)	−349.28019
TS5	−14.5 (14.9)	−349.26255
TS6	−31.0 (15.8)	−349.28884
13+MeOH	0.0	−465.03790
16	−11.7	−465.05658
17	−10.9	−465.05524
18	−21.3	−465.07190
TS7	−10.4 (1.3)[b]	−465.05444

[a] Values in parentheses are activation energies.
[b] Energy relative to that of **16**.

coordinates (IRC)[13] calculations, we checked that all the obtained TSs connected reactants and products at the RHF/6-31G level of theory (ab initio molecular orbital calculations). Moreover, IRC calculations at the B3LYP/6-31G** level of theory were carried out to refine reaction and energy profiles for Paths 2 and 4 which are the key routes to determine the product distribution observed.

Results and Discussion

Reaction mechanism of indane formation (Paths 1 and 4)

A hydride first migrates from the γ-carbon C(9) in the propyl side chain to the cationic carbon C(1) in **10**. Although this migration may yield the cation intermediate **11** in Path 1, no geometry of the primary cation was optimized. Then, we tried to obtain **TS1**[14] which connects **10** and **15**. The obtained TS (**TS4**) has the C(6)–C(9) and the C(1)–C(9) which are 1.967 and 2.225 Å in length.

In order to confirm that the TS connects **10** and **15**, the IRC calculations were performed at the B3LYP/6-31G** level of theory. Fig. 3 displays the energy profile and the geometry transformation along the IRC.[15]

When the reaction proceeds forward from s=0.0 (TS) to s=5.99 amu$^{1/2}$ Bohr, the C(9) moves towards the C(1). The geometry change accompanies decrease of the dihedral angle τ[C(1)–C(6)–C(7)–C(8)]: 61.6°, 41.9° and 32.6° at TS, s=2.99 and 5.99 amu$^{1/2}$ Bohr, respectively. The C(1)–C(9) bond appears at s=5.99 amu$^{1/2}$ Bohr because of being 1.617 Å in length. Formation of **15** is almost complete at this point on the IRC. When the reaction proceeds in reverse from s=0.00 to s=−4.98 amu$^{1/2}$ Bohr, the obtained TS changes its geometry not to **11** with an open chain but to a phenonium ion **12** with a four-membered ring. Therefore, the obtained geometry is the **TS4** which connects **15** and **12** (Path 4). The primary cation such as **11** is too unstable to exist in the gas phase. Path 1 is the route which produces not **11** but **12** probably with a negligible barrier although no TS structure was obtained.

In the optimized structure of **12** (Fig. 2) at the B3LYP/6-31G** level, the C(6)–C(7) (1.634 Å) is equal to the C(6)–C(9) in length and the four-membered ring is perpendicular to the benzene ring, that is, the dihedral angle between the two rings was calculated to be 90.5°. **12** turned out to be more stable by 29.4 kcal mol^{-1} than **10** and the activation energy through the **TS4** was evaluated to be only 3.8 kcal mol^{-1}. It was gathered that immediately after the formation of **10**, a hydride of the γ-position migrates to form a new C(1)–H bond, followed by formation of **12** with a spiro-type fragment (Path 1). **12**, in turn, easily isomerizes to an intermediate with a five-membered ring **15** and then **3** is formed (Path 4).

Formation of intermediate 13 (Paths 2 and 5)

There are two routes which produce the cation intermediate **13** as shown in Fig. 1. One includes a hydride transfer from C(8) to C(9) in **12** (Path 5) via **TS5**. The B3LYP/6-31G** level of theory estimated the activation energy to be 14.9 kcal mol^{-1}. This barrier is higher by 11.1 kcal mol^{-1} than the corresponding value for Path 4 as discussed above. Therefore, all of **12** formed leads to the intermediate **15** and Path 5 is ruled out.

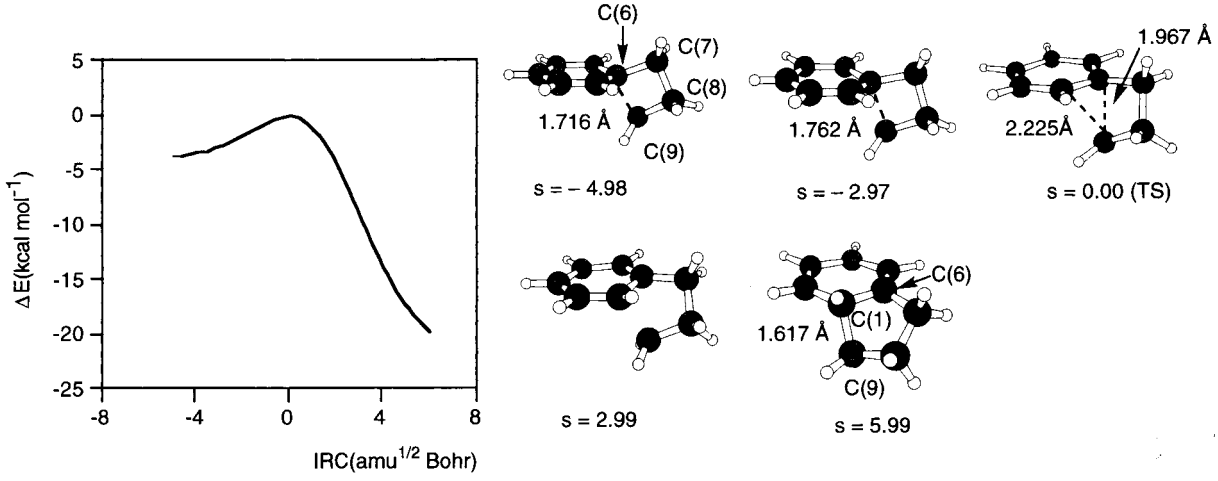

Figure 3. Potential energy profile and geometry transformation along the IRC from **12** to **15** (Path 4).

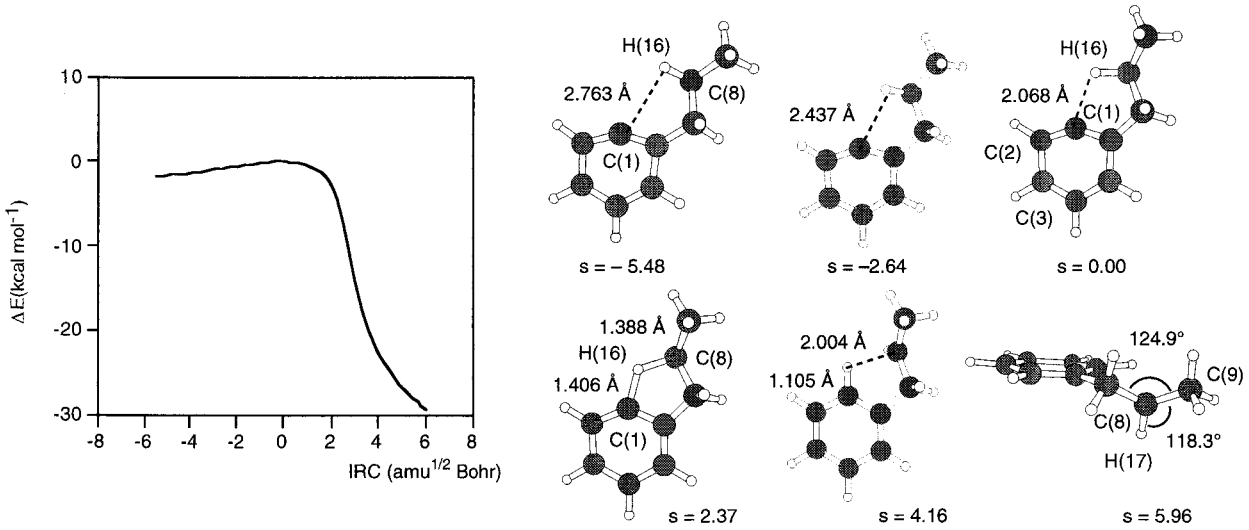

Figure 4. Potential energy profile connecting **10** with **13** (Path 2) together with geometry transformation along the IRC.

The other route is Path 2 which forms **13** directly from **10**. In this route, C(1) in **10** accepts a hydride from the β-carbon C(8) in the propyl side chain through **TS2**. Fig. 4 displays a potential energy profile and a geometry transformation along the IRC of Path 2 at the B3LYP/6-31G** level. The potential energy gradually increases from $s=-5.48$ amu$^{1/2}$ Bohr to the TS, and then drops sharply after $s=2.00$ amu$^{1/2}$ Bohr. The activation energy was estimated to be only 1.2 kcal mol^{-1} and thus, **13** is mainly formed through this route. This intermediate is the precursor of the products **6** and **9**.

The C(1)–H(16) length is 2.763 Å at $s=-5.48$ amu$^{1/2}$ Bohr. The dihedral angle τ[H(16)–C(1)–C(2)–C(3)] at the TS turned out to be 179.7°. The H(16) locates on the same plane of the benzene ring to facilitate interaction between its s-orbital and the empty p-orbital of C(1). A five-membered ring is formed at $s=2.37$ amu$^{1/2}$ Bohr with the C(8)–H(16) and the C(1)–H(16) which are 1.388 and 1.406 Å in length. The C(8)–H(16) bond breaks and a new C(1)–H(16) bond formation is almost complete at $s=4.16$ amu$^{1/2}$ Bohr since these lengths are 2.004 and 1.105 Å at this point. As the ∠H(17)–C(8)–C(9) and ∠C(7)–C(8)–C(9) angles at $s=5.96$ amu$^{1/2}$ Bohr are 118.3° and 124.9°, respectively, C(8) takes almost sp^2 hybridization with an empty p-orbital. The orbital can interact with occupied π-orbitals in the benzene ring. This interaction leads to forming a three-membered ring in **13** although the C(6)–C(8) length is as long as 1.765 Å. This is a reason why **13** is much more stable by 46.8 kcal mol^{-1} than **10**. Loss of a proton of the γ-carbon in **13** results in forming **8**, which does not come from **11** since the primary cation is ruled out as discussed above.

Formation of benzyl cation 14 (Paths 3 and 6)

The cation **14** turned out to be more stable than **10** by 55.8 kcal mol^{-1} because it is a benzyl cation with conjugation between an empty p-orbital of the α-carbon and π-orbitals in the benzene ring. There are two feasible paths which lead to forming the benzyl intermediate. One is Path 3 where the C(1) in **10** directly abstracts a hydride from the α-carbon to form **14**. The activation energy of this path was estimated to be 19.3 kcal mol^{-1}. Such a high activation energy is ascribed to the geometry of the **TS3** with the strained four-membered ring, which is required in transferring a hydride from the α-carbon C(7) to C(1) as shown in Fig. 2. This barrier is much higher than those for Paths 1 and 2. Therefore, all the phenyl cations go to form **12** or **13**.

The other is Path 6 where a hydride H(15) of the C(7) in **13** moves to the C(8) via **TS6**. However, this reaction has to overcome a barrier as high as 15.8 kcal mol^{-1}. This barrier should be higher than that when the reaction forms the solvolysis product **6** from the intermediate **13**. Therefore, neither Path 3 nor Path 6 explains formation of **14**.

The product analysis indicated that the major product of the photosolvolysis of **1** is **5** (27%). The precursor of **5** is the benzyl cation **14** although the present calculations ruled out the two feasible routes in Scheme 1. We have to consider an alternative route in order to explain the observed product distribution.

Solvent assisted mechanism (Path 7)

There are several examples of solvent molecules assisting the migration of proton and reducing activation barriers of reactions.[16] It is also possible to draw the mechanism in which a solvent assists conversion of **13** to **14**, i.e. a multi-step mechanism (Path 7) represented in Eqs. (2) and (3).

$$\mathbf{13} + CF_3CH_2OH \rightarrow \mathbf{9} + CF_3CH_2OH_2^+ \quad (2)$$

$$\mathbf{9} + CF_3CH_2OH_2^+ \rightarrow \mathbf{14} + CF_3CH_2OH \quad (3)$$

Once **13** is formed, the reaction producing the solvolysis product **6** competes with Path 7 as shown in Scheme 2. In the present reaction, a trace of **9** in the products is a key to understanding formation of **5**. In order to analyze this

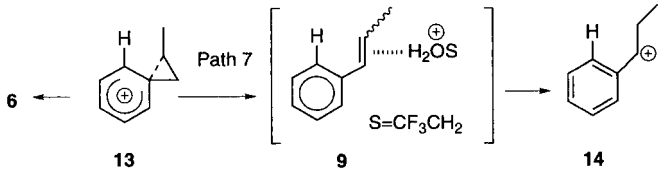

Scheme 2.

mechanism, CH_3OH was adopted as a model of TFE for the purpose of simplifying calculations. Fig. 5 displays the energy profile of the mechanism together with optimized structures.

First of all, a weak interaction between the oxygen O(21) in CH_3OH and the H(15) of the α-carbon of **13** make it possible to form a complex **16**. The H(15)–O(21) distance was calculated to be 2.262 Å. This hydrogen bond stabilizes **16** by 11.7 kcal mol^{-1}. Then, methanol abstracts H(15) in proton to form the second complex **17** which consists of **9** and $CH_3OH_2^+$ ion.[17] The H(15)–O(21) bond length in the oxonium ion moiety is 1.069 Å. The H(15) interacts with the π-orbital of the C(7)–C(8) bond because the H(15)–C(7) and H(15)–C(8) distances are 1.887 and 1.840 Å, respectively. This complex is less stable by 0.8 kcal mol^{-1} than **16**.

In the third step, migration of a proton from the $CH_3OH_2^+$ to the styrene fragment produces **18** and the reaction proceeds through **TS7**. The C(8)–H(15) and the H(15)–O(21) distances of the TS are 1.520 and 1.185 Å, respectively. As the dihedral angle τ[C(6)–C(7)–C(8)–H(15)] is 57.8°, the H(15) interacts with π-orbital of the C(7)–C(8) bond. In the complex **18**, **14** interacts weakly with a methanol since the H(16)–O(21) distance is 2.141 Å. The activation energy of the path through the **TS7** was calculated to be only 0.5 kcal mol^{-1}. Thus, the total activation barrier of the isomerization from **16** to **18** is as low as 1.3 kcal mol^{-1}. All the molecules related to Path 7 are more stable than isolated **13**+MeOH. Because of the stability of the related molecules in this route, **13** is predominantly converted to **14** via the solvent assisted mechanism. It is necessary to note that TFE instead of methanol was used in our experiments. The barrier height calculated for Path 7 is considered to be higher than that of the present calculations since the basicity of TFE is less than that of methanol.

McClelland and coworkers reported that a laser flash photolysis of *p*-methoxystyrene in TFE produced trifluoroethanol adducts, which are similar to that obtained in our experiment. Enhanced basicity of the photoexcited styrene derivative makes it possible to extract a proton of TFE to form *p*-methoxyphenylethyl cation.[18] Therefore, it is possible to consider an alternative path where **9**, obtained through the reaction of Eq. (2), is photoexcited and extracts a proton to form **14** in TFE. It is not necessary to consider **TS7** in this mechanism.

The existence of **9** is the key for the observation that the product ratio of **5** (27%) is larger than that of **6** (12%).

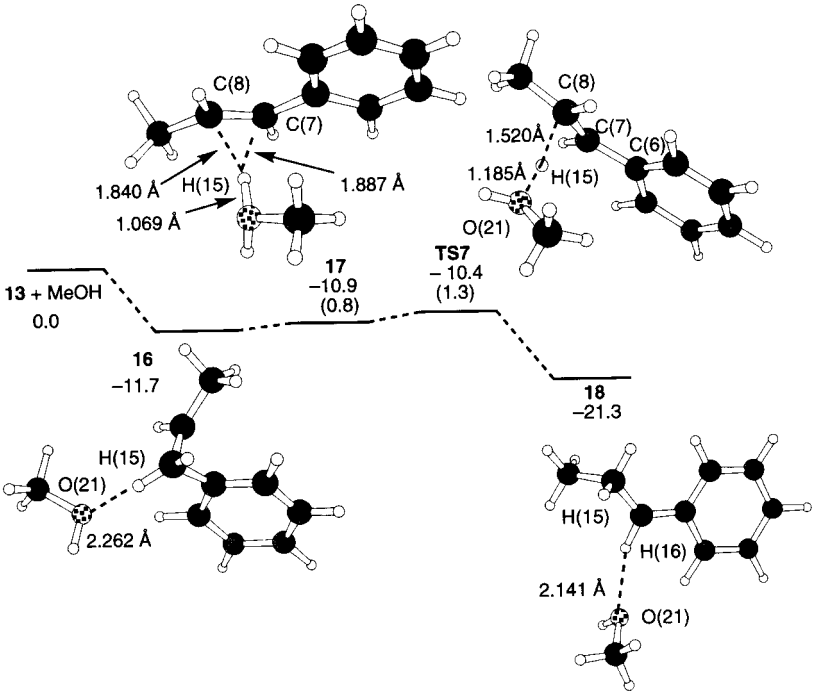

Figure 5. Energy-level profile for the solvent assisted mechanism of proton transfer (Path 7) with the optimized structures of the related molecules. Values in parentheses are energies relative to that of **16**.

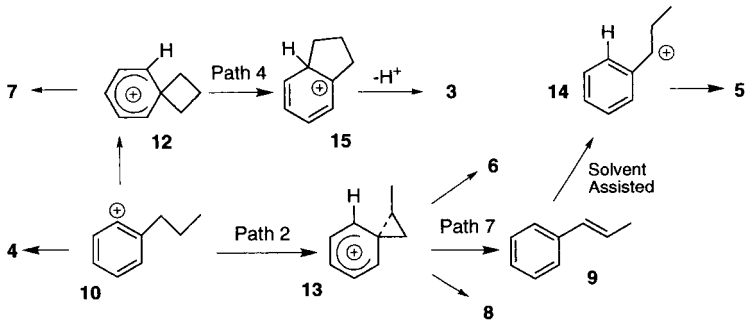

Scheme 3.

Concluding Remarks

The key of Scheme 1 is formation of the phenyl cation intermediate **10**. Our DFT calculations show the possibility that three routes consume the formed intermediates which are summarized in Scheme 3. The first is the route where the intermediate reacts with a solvent to form **4** (12%). The second is the route where the positive charge on the C(1) moves to the γ-position of the side chain, followed by formation of the intermediate **12**. This unstable intermediate quickly changes its form to **7** (trace) or **3** (8%) via **15**.

The last is the path which produces the intermediate **13** with a three-membered ring and forms the products, **5** (27%), **6** (12%), **8**(5%) and **9** (trace). Therefore, the last route is the major path of the photosolvolysis of **1**. While the C(1) of **10** in the second route has to abstract the hydride of the γ-carbon, that of the third one abstracts a hydride of the β-carbon. The hydride of the γ-carbon occupies a position far from the cation center C(1). This is the reason why the third is the main route of the present photosolvolysis.

We assume the phenyl cation as an intermediate of photosolvolysis of 2-chloropropylbenzene and draw the scheme with reaction paths which explain all the products obtained. A solvent played an important role in producing the main solvolysis product **5**. Therefore, the present DFT calculations strongly suggest the existence of the phenyl cation for the photosolvolysis of **1** in TFE although the intermediate is too unstable to detect experimentally.

Acknowledgements

The authors thank the Computer Center, Institute for Molecular Science at the Okazaki National Research Institutes for the use of the NEC HSP computer and Library Program gaussian94. This study was also supported in part by the Grant-In-Aid (Molecular Physical Chemistry, No. 11166249) from the Ministry of Education, Sports and Culture and in part by the Hayashi Memorial Foundation for Female Natural Scientists.

References

1. Beauchamp, J. L. *Adv. Mass Spectrom.* **1974**, *6*, 717.
2. (a) Dill, J. D.; Schleyer, P. v. R.; Binkley, J. S.; Seeger, R.; Pople, J. A.; Haselbach, E. *J. Am. Chem. Soc.* **1976**, *98*, 5428. (b) Dill, J. D.; Schleyer, P. v. R.; Pople. *J. Am. Chem. Soc.* **1977**, *99*, 1. (c) Castenmiller, W. A. M.; Buck, H. M. *Recl. Trav. Chim. Pays-Bas* **1977**, *96*, 207. (d) Vincent, M. A.; Radom, L. *J. Am. Chem. Soc.* **1978**, *100*, 3306. (e) Gamba, A.; Simonetta, M.; Suffritti, G.; Szele, I.; Zollinger, H. *J. Chem. Soc., Perkin Trans. 2* **1980**, 492. (f) Alcock, N. W.; Greenhough, T. J.; Hirst, D. M.; Kemp, T. J.; Payne, D. R. *J. Chem. Soc., Perkin Trans. 2* **1980**, 8. (g) Tasaka, M.; Ogata, M.; Ichikawa, H. *J. Am. Chem. Soc.* **1981**, *103*, 1885. (h) Schleyer, P. R.; Kos, A. J.; Raghavachari, K. *J. Chem. Soc., Chem. Commun.* **1983**, 1296. (i) Butcher, V.; Costa, M. L.; Dyke, J. M.; Ellis, A. R.; Morris, A. *Chem. Phys.* **1987**, *115*, 261. (j) Bernardi, F.; Grandinetti, F.; Guarino, A.; Robb, M. A. *Chem. Phys. Lett.* **1988**, 309. (k) Schleyer, P. v. R.; Jiao, H.; Glukhotsev, M. N.; Chandrasekhar, J.; Kraka, E. *J. Am. Chem. Soc.* **1994**, *116*, 10129. (l) Apeloig, Y.; Müller, T. In *Dicoordinated Carbocations*; Rappoport, Z., Stang, J. P., Eds.; Wiley: Chichester, 1997, p 9.
3. Reviews: (a) Zollinger, H. *Acc. Chem. Res.* **1973**, *6*, 335. (b) Zollinger, H. *Angew. Chem. Res.* **1978**, *90*, 151. (c) Hegarty A. F. In *The Chemistry of Diazonium and Diazo Groups*; Patai, S., Ed.; Wiley: London, 1978; p 511. (d) Zollinger, H. In *The Chemistry of Triple-bonded Functional Groups*; Patai, S., Rappoport, Z., Eds.; Wiley: London, 1983; Suppl. C, p 603. (e) Zollinger, H. *Pure Appl. Chem.* **1983**, *55*, 401.
4. Martinson, P. *Acta Chem. Scand.* **1968**, *22*, 1357.
5. Sikkar, R.; Martinson, P. *Acta Chem. Scand. B* **1980**, *34*, 551.
6. (a) Streitwieser, A.; Dafforn, A. *Tetrahedron Lett.* **1976**, 1435. (b) Subramanian, L. R.; Hanack, M.; Chang, L. W. K.; Imhoff, M. A.; Schleyer, P. v. R.; Effenberger, F.; Kurtz, W.; Stang, P. J.; Dueber, T. E. *J. Org. Chem.* **1976**, *41*, 4099. (c) Laali, K.; Szele, I.; Yoshida, K. *Helv. Chim. Acta* **1983**, *66*, 1710.
7. (a) Himeshima, Y.; Kobayashi, H.; Sonoda, T. *J. Am. Chem. Soc.* **1985**, *107*, 5286. (b) Apeloig, Y.; Arad, D. *J. Am. Chem. Soc.* **1985**, *107*, 5285.
8. (a) Angelini, G.; Speranza, M.; Segre, A. L.; Altman, L. J. *J. Org. Chem.* **1980**, *45*, 3291. (b) Speranza, M. *Tetrahedron Lett.* **1980**, *21*, 1983. (c) Angelini, G.; Fornarini, S.; Speranza, M. *J. Am. Chem. Soc.* **1982**, *104*, 4773. (d) Speranza, M.; Keheyan, Y.; Angelini, G. *J. Am. Chem. Soc.* **1983**, *105*, 6377. (e) Angelini, G.; Sparapani, C.; Speranza, M. *Tetrahedron* **1984**, *40*, 4865. (f) Colosimo, M.; Speranza, M.; Cacace, F.; Ciranni, G. *Tetrahedron* **1984**, *40*, 4873. (g) Speranza, M. *Chem. Rev.* **1993**, *93*, 2933. (h) Speranza, M. In *Dicoordinated Carbocations*; Rappoport, Z., Stang, J. P., Eds.; Wiley: Chichester, 1997; p 157 and references cited therein.
9. Reviews: (a) Cornelisse, J.; Lodder, G.; Havinga, E. *Rev. Chem. Intermed.* **1979**, *2*, 231. (b) Párkányi, C. *Pure Appl. Chem.* **1983**, *55*, 331. (c) Cornelisse, J. In *CRC Handbook of Organic Photochemistry and Photobiology*; Horspool, W. M., Song, P. S., Eds.; CRC Press: Boca Raton, 1995; p 250. (d) Lodder, G.; Cornelisse, J.

In *The Chemistry of Halides, Pseudo-halides and Azides*; Patai, S., Rappoport, Z., Eds.; Wiley: London, 1995; Suppl. D2, p 861.
10. Yamazaki, S.; Sonoda, T.; Harada, M.; Hori, K. Proceedings of Kyushu International Symposium on Physical Organic Chemistry, KISPOC-VI, Fukuoka, 1995; p 257.
11. Frisch, M. J.; Trucks, G. W.; Schlegel, H. B.; Gill, P. M. W.; Johnson, B. G.; Robb, M. A.; Cheeseman, J. R.; Keith, T. A.; Petersson, G. A.; Montgomery, J. A.; Raghavachari, K.; Al-Laham, M. A.; Zakrzewski, V. G.; Ortiz, J. V.; Foresman, J. B.; Cioslowski, J.; Stefanov, B. B.; Nanayakkara, A.; Challacombe, M.; Peng, C. Y.; Ayala, P. Y.; Chen, W.; Wong, M. W.; Andres, J. L.; Replogle, E. S.; Gomperts, R.; Martin, R. L.; Fox, D. J.; Binkley, J. S.; Defrees, D. J.; Baker, J.; Stewart, J. P.; Head-Gordon, M.; Gonzalez, C.; Pople, J. A. gaussian94, Revision A.1; Gaussian, Inc., Pittsburgh, PA, 1995.
12. Hehre, W. J.; Ditchfield, R.; Pople, J. A. *J. Chem. Phys.* **1972**, *56*, 2257.
13. (a) Head-Gordon, M.; Pople, J. A. *J. Chem. Phys.* **1988**, *89*, 5777. (b) Fukui, K. *Acc. Chem. Res.* **1981**, *14*, 363.
14. The number denoted for TS corresponds to that of the reaction path. For example, **TS1** indicates the TS for Path 1.
15. 's' in amu$^{1/2}$ Bohr unit is the distance from the TS, showing how a geometry along the IRC is different from the TS geometry.
16. (a) Yamazaki-Nishida, S.; Cervera-March, S.; Nagano, K. J.; Anderson, M. A.; Hori, K. *J. Phys. Chem.* **1995**, *99*, 15814. (b) Nagaoka, M.; Okuno, Y.; Yamabe, T. *J. Am. Chem. Soc.* **1991**, *113*, 769. (c) Johnson, B.; Karlstrom, G.; Wennerstrom, H. *J. Am. Chem. Soc.* **1978**, *100*, 1658.
17. The TS structure which connects **16** and **17** was not obtained. Even if the TS exists, its energy cannot be much higher than **17**.
18. (a) McClelland, R. A.; Kanagasabapathy, V. M.; Steenken, S. *J. Am. Chem. Soc.* **1998**, *110*, 6913. (b) McClelland, R. A.; Cozens, F.; Steenken, S. *Tetrahedron Lett.* **1990**, *31*, 2821.